Helicity of the Photospheric Magnetic Field

Alexei A. Pevtsov, Richard C. Canfield

Department of Physics, Montana State University, Bozeman

Observations of vector magnetic fields from various observatories have been used to study the current helicity of the solar magnetic field, computed either as the ratio α_z of the vertical components of the electric current density J_z to the magnetic induction B_z or the force-free field α coefficient. Low resolution full disk longitudinal magnetograms have also been used to reconstruct the large-scale vector magnetic field and compute $H_c = B_z \cdot (\nabla \times B)_z$.

All these studies show a hemispheric helicity rule – the photospheric magnetic field in the northern/southern hemisphere has negative/positive current helicity. It appears, however, that the hemispheric asymmetry rule is weak. Carrington maps of H_c show that areas of both signs of current helicity are present in each hemisphere. In the Mees and Huairou data one sees a tendency for active regions that disobey the hemispheric helicity rule to originate in certain longitudes for many solar rotations.

We discuss the possible origin of the hemispheric helicity rule and conclude that neither differential rotation, nor the Coriolis force can fully explain the observations for following reasons. First, the hemispheric helicity rule is weak. Second, there is the pattern of helicity within active region. Third, a correlation between magnetic field twist and the tilt of active region is an opposite in sign to what one should expect from the Coriolis force action.

1. INTRODUCTION

Hale [1927] studied chromospheric H_α vortices around sunspots and found that they form counterclockwise spirals north of the equator and clockwise spirals south of it, independent of the solar cycle. Later *Richardson* [1941] confirmed this result on a larger dataset of more than 140 active regions. Although both *Hale* and *Richardson* explained their results in terms of solar atmospheric circulation, it is believed now that the chromospheric vortices reflect the hemispheric helicity rule for the magnetic field, discovered only recently [*Seehafer*, 1990; *Martin et al.,* 1994; *Pevtsov et al.,* 1995], and not yet fully understood. It has alternatively been ascribed to either photospheric [*Zirker et al.,* 1997; *vanBallegooijen et al.,* 1998] or subphotospheric [*Rust and Kumar*, 1994; *Longcope et al.,* 1998] processes.

Seehafer [1990] studied the sign of the force-free field coefficient α of 16 active regions and found hemispheric asymmetry. *Pevtsov et al.* [1995] computed α for 69 active regions and found that 76% of the regions in the northern hemisphere have negative α, and 69% in the southern hemisphere, positive. Later the tendency was confirmed in other independent datasets [*Abramenko et al.,* 1997; *Bao and Zhang*, 1998; *Longcope et al.,* 1998]. The hemispheric helicity rule has also been observed in the interplanetary magnetic field [*Matthaeus et al.,* 1999], chromospheric filaments [*Martin et al.,* 1994; *Rust*, 1999] and sheared coronal loops [*Rust and Kumar*, 1996; *Canfield and Pevtsov*, 1999].

2. MEASURES OF HELICITY

It is widely believed now that the solar magnetic field is generated by a dynamo operating at the base of the convection zone. The flux generated there is buoyant and rises to the surface as Ω-shaped loops whose ends are anchored in the convectively stable core. Where it intersects the photosphere, the Ω loop forms a solar active region with sunspots of opposite polarity connected through the corona [*Babcock*, 1961]. The thin flux tube model has been used in several studies of Ω loops rising through the convective zone [*Fisher et al.,* 1995] and interacting with turbulent convection [*Longcope et al.,* 1999].

2.1. Thin Flux Tube

Consider a thin flux tube T defined by axial $B_a = \{0, 0, B_z(r)\}$ and meridional $B_m = \{0, B_\theta(r), 0\}$ components and $\mathbf{B}(x) = \nabla\times\mathbf{A}(x)$ in a domain $\mathcal{D}$ on whose surface $n\cdot\mathbf{B} = 0$. Under these circumstances the magnetic helicity $\mathcal{H} = \int_{\mathcal{D}} \mathbf{A}\cdot\mathbf{B}dV = \int_T \mathbf{A}_a \cdot \mathbf{B}_a dV + 2\int_T \mathbf{A}_m \cdot \mathbf{B}_m dV$, where first integral represents twist $\mathcal{T}$ and second represents writhe $\mathcal{W}$ [*Moffatt and Ricca*, 1992]. In absence of dissipative processes the magnetic helicity is a conserved quantity [*Field*, 1986].

Only the density of twist in the photosphere can be measured using vector magnetograms. The writhe can be studied independently, using the shape of coronal loops above solar active regions [*Pevtsov et al.,* 1997; *Canfield and Pevtsov*, 1999].

2.2. Helicity Proxies

Existing solar vector magnetographs measure three components of the magnetic field $\mathbf{B} = \{B_x, B_y, B_z\}$ at a single level in solar atmosphere. Strictly speaking, neither the magnetic vector potential, nor the magnetic helicity can be computed from these data without additional assumptions, since the measurements are local, but these quantities are global.

2.2.1. Force-free field α. Consider a force free magnetic field $\nabla\times\mathbf{B} = \alpha\mathbf{B} = \mu\mathbf{J}$, where B - magnetic induction, μ - magnetic permeability in vacuum, J - electric current density. For a linear force-free field with $\alpha \equiv const$, the magnetic vector potential $A = \alpha^{-1}B + \nabla\Psi$, where Ψ is arbitrary scalar function and $\mathcal{H} = \int_{\mathcal{D}}(\alpha^{-1}B + \nabla\Psi)BdV = 2\mu\alpha^{-1}E_m$. Magnetic energy E_m can be computed using the virial theorem [Priest, 1984] $E_m = \mu^{-1}\int_S(xB_x - yB_y)B_z dxdy$. Values of α that best fit an entire active region have been used by *Seehafer* [1990], *Pevtsov et al.* [1995] and *Hagyard et al.* [1998] to study the hemispheric helicity rule (Section 4).

For a non-linear force-free field $\alpha = \alpha(x,y)$ and $\alpha_z(x,y) = (\nabla \times B)_z/B_z = (\frac{\partial B_y}{\partial x} - \frac{\partial B_x}{\partial y})\frac{1}{B_z}$. This approach has been used to study local helicity patterns in active regions [*Pevtsov et al.,* 1994], Section 5.

2.2.2. Current helicity. Alternatively, one can compute the current helicity $H_c = \mathbf{B}(\nabla \times \mathbf{B})$. In general, only $(\nabla \times \mathbf{B})_z$ can be derived from a vector magnetogram; for a force-free field $(\nabla \times \mathbf{B})_x = (\nabla \times \mathbf{B})_y = (\nabla \times \mathbf{B})_z$. *Seehafer* [1990] showed that for a cylindrically symmetric infinite flux tube current helicity has the same sign and increases/decreases as the magnetic helicity does. For a linear force-free field $H_c = \alpha \cdot B^2 = \alpha^2 H_m$, where H_m is the magnetic helicity density.

H_c averaged over a whole active region has been used to study the hemispheric helicity rule [*Abramenko et al.,* 1997; *Bao and Zhang*, 1998] and the large-scale pattern of helicity [*Pevtsov and Latushko*, 1995], Section 6.

3. OBSERVATIONAL ASPECTS

3.1. Vector Magnetographs

The results of studies that we review in this paper are based on observations from several vector magnetographs including the Haleakala Stokes Polarimeter (HSP) [*Mickey*, 1985] , Advanced Stokes Polarimeter (ASP) [*Lites et al.,* 1993], Huairou Solar Station (HSS) vector magnetograph [*Bao and Zhang*, 1998] and Marshall Space Flight Center (MSFC) magnetograph [*Hagyard et al.,* 1985]. The differences between the instruments in observational technique and data reduction can effect helicity observations.

Both HSP and ASP derive magnetic field vector from full Stokes profiles of two spectral lines Fe I $\lambda\lambda$ 6301.5 and 6102.5, using a nonlinear least-squares Unno profile-fitting routine [*Skumanich and Lites*, 1987]. It is important to note that the method makes a first-order correction for the magneto-optical effects (Faraday rotation) and magnetic filling factor.

In contrast, the MSFC and HSS instruments take polarization measurements in a single fixed position of a spectral line profile (MSFC can make successive observations in several points across a spectral line). The value of **B** is then determined via comparison of the measured polarizations with theoretical ones, computed using a model of the solar atmosphere [*Semel et al.*, 1991]. The use of limited spectral information makes the MSFC and HSS magnetographs potentially susceptible to several known problems: magnetic saturation, under-resolution, and Faraday rotation. Recently, *Hagyard et al.* [1998] investigated the role of these factors on helicity computation using the MSFC magnetograph data. We are unaware of a similar study involving HSS data.

3.1.1. Magnetic saturation. The magnetic saturation is the result of nonlinear dependence between field strength and measured polarization. Thus, beginning with certain field strength polarization may vary very little or even decrease, although the field strength will continue to increase. The saturation alters both total field strength and the direction of transverse field and hence is important for helicity computation. However, *Hagyard et al.* [1998] concluded that careful choice of a threshold in the transverse field eliminates saturated pixels from α calculations. On the other hand, it is difficult if possible to correct for the saturation effect in the computation of α_z and H_c.

3.1.2. Under-resolution. Solar photospheric magnetic fields are concentrated in the small flux tubes, whose cross-sections are far below the spatial resolution limits of existing magnetographs [*Stenflo*, 1994]. Adequate spectral resolution and sampling allows one to determine the relative contribution to the radiation from the magnetized and non-magnetized plasma to first order. In the MSFC and HSS magnetographs this information is lost. Lack of such information about the magnetic filling factor leads to underestimation of the field strength and may distort the local helicity pattern. However, *Hagyard et al.* [1998] compared α from HSP and MSFC vector magnetograms for three active regions and found that they are in good agreement in spite of the magnetic filling factor uncertainty.

3.1.3. Faraday rotation. *West and Hagyard* [1983] found that the Faraday rotation can change the azimuth of the transverse field by as much as 45° for measurements taken near the center of a spectral line or in the far wing. In a magnetic field of uniform polarity the azimuths of the transverse field will rotate in the same direction. Thus, Faraday rotation mimics $\nabla \times B$ and hence may effect significantly the computation of helicity. However, *Hagyard et al.* [1998] concluded that the effect of Faraday rotation on the α computation is relatively unimportant for the MSFC dataset, since the measurements are usually taken far enough in the wing of a spectral line. On the other hand, they found a strong indication of the Faraday rotation in HSS data, at least in one case of a single active region they have analyzed. One could expect it, since the HSS magnetograph measures transverse field in the center of a spectral line, where the Faraday rotation is maximum.

3.2. Full Disk Longitudinal Magnetograms

In Section 2 we have defined two helicity proxies, which one can compute using vector magnetograms. This approach, however, limits the helicity studies to the solar active regions, since the observations of the vector magnetic field for the full solar disk are unavailable at present time. To overcome this limitation *Pevtsov and Latushko* [1995] employed a reconstruction technique [*Grigoriev and Latushko*, 1992] to compute vector magnetic field from a set of longitudinal magnetograms. The method works under assumption that the large-scale magnetic field evolves slowly and that all changes of B_{long} are the result of changing projection angle. *Latushko and Pevtsov* [1998] applied this technique to longitudinal magnetograms from Wilcox Solar Observatory (WSO) and Michelson Doppler Imager (MDI, SOHO spacecraft). Section 6.2 describes some of their results.

4. HELICITY OF ACTIVE REGION MAGNETIC FIELDS

4.1. Hemispheric Helicity Rule

Since the magnetic pressure in the photosphere is comparable with the gas pressure, the magnetic field in the photosphere is not force-free [*Priest*, 1984]. However, the force-free field assumption has been widely used to extrapolate the magnetic field from the photosphere up to the corona [*Semel et al.*, 1991]. Using α – a by-product of these calculations – *Seehafer* [1990] noticed a hemispheric asymmetry in the distribution of sign of α: negative in the northern hemisphere and positive in the southern. *Pevtsov et al.* [1995] studied 69 active regions and established the hemispheric helicity rule on $\sim$ 70%/30% level, although the extended HSP dataset [*Longcope et al.*, 1998] shows the tendency on $\sim$ 60%/40% level (Table 1). Table 1

Figure 1 shows the latitudinal distribution of α_{best} for all 203 active regions of the *Longcope et al.* [1998] dataset. Figure 1

Two other groups studied the current helicity density of active regions by averaging H_c over whole region. *Abramenko et al.* [1997] examined 40 active regions and confirmed the hemispheric helicity rule on the same level as *Pevtsov et al.* [1995]. *Bao and Zhang* [1998] studied 421 active regions and found a stronger 80%/20% tendency.

Although the hemispheric helicity rule was established for solar cycle 22, observations show the same sign of the hemispheric asymmetry in solar cycles 21 [*Hagyard et al.*, 1998] and 23 [*Bao and Zhang*, 1998].

The current helicity of the large-scale magnetic field also reveals the same hemispheric asymmetry. Using MDI full disk magnetograms *Latushko and Pevtsov* [1998] reconstructed vector magnetic field in the Carrington coordinate grid for one solar rotation (June-July 1996, Carrington rotation number CRN 1910). Averaging radial B_r and toroidal B_λ components of the magnetic vector over all longitudes λ for each latitude φ, they were able to compute the latitudinal profile of the current helicity $H_c = \frac{(\nabla \times B)_r}{B_r} B^2$, where $(\nabla \times B)_r = \frac{1}{r \sin\varphi}(\frac{\partial}{\partial\varphi}(\sin\varphi \cdot B_\lambda) - \frac{\partial B_\varphi}{\partial\lambda})$ and $\frac{\partial B_\varphi}{\partial\lambda} \equiv 0$, as the result of longitudinal averaging. Figure 2 shows the latitudinal profile of H_c from *Latushko and Pevtsov* [1998]. The large-scale magnetic field has predominantly negative/positive current helicity density in northern/southern hemisphere. It is important to note significant variations of H_c in low latitudes, where the sunspot activity is large, and much smaller H_c variations in high latitudes, with no sunspot activity. The current helicity increases toward poles, a feature that can not be seen in active region data. The large variations of H_c between $\sim \pm 30°$ can be the result of the large-scale helicity areas described in Section 6.

Figure 2

Duvall et al. [1979] used WSO low resolution magnetograms to compute latitudinal profiles of the vertical components of large-scale magnetic field and electric currents crossing the photosphere. Comparing these two profiles we find the same hemispheric helicity rule as in Figs. 1 and 2.

4.2. Tilt-Twist Correlation

The relationship between the two components of magnetic helicity can be used to discriminate between different origins of helicity. Consider helicity conservation in a flux tube with zero helicity. Twisting modifies both twist $\mathcal{T}$ and writhe $\mathcal{W}$ in the tube. However, the writhe will be opposite in sign to the twist. On the other hand, consider a highly twisted tube. It may "trade" its twist for writhe, again conserving total (non-zero) helicity. In a first case, $\mathcal{T}$ and $\mathcal{W}$ will be opposite in sign; in a second case they will have same sign. In the photosphere we can study a relationship between the internal twist of the magnetic field represented by α_{best} and the writhe represented by "tilt" of a solar active region (Joy's law, [*Zirin*, 1988]), the angle between N-S axis of the region and solar equator. It is believed that such tilt arises due to the Coriolis force acting on plasma flowing away from the apex of rising Ω-loop [*Fisher et al.*, 1995]. As a result of helicity conservation, one should expect a strong correlation between twist (α_{best}) and writhe (tilt), assuming that the Ω-loop was originally untwisted, and is in equilibrium.

For 99 active regions from Haleakala Stokes Polarimeter datatset *Canfield and Pevtsov* [1998] computed both α_{best} and tilt per unit length (θ/L). They defined θ to be positive in counterclockwise direction, so that $\theta > 0$ corresponds $\mathcal{W} < 0$ (negative writhe) and *vise versa.* To guide the analysis, *Canfield and Pevtsov* used a simple non-linear force-free field – a uniformly twisted cylindrical flux tube [*Priest*, 1984]. It is straightforward to show that for this field (which has no writhe), $\alpha_{best} = \mathcal{T}/L$, where the separation between sunspots of opposite polarity is used as a measure of L. Figure 3 shows a relationship between θ/L and α_{best}. Clearly, the data do not show a positive correlation between twist and and tilt, as one would expect if the Coriolis force had produced twist in originally untwisted flux tubes. In fact, there is a weak anticorrelation between α_{best} and θ/L, which implies that the writhe and twist density at the photosphere have the same sign!

Figure 3

5. HELICITY PATTERNS WITHIN ACTIVE REGIONS

In the previous section we presented observational results based on representation of each active region by a single parameter. Although this approach has been proven to be useful in study of the hemispheric helicity rule, it ignores the small-scale patterns of oppositely directed currents which are known to exist inside active regions [*Gary et al*, 1987; *Pevtsov and Peregud*, 1990].

Pevtsov et al. [1994] described such patterns of α_z which they found to persist for several days, with a characteristic decay time $\tau \sim 27$ hours. It has been convincingly argued, albeit in a limited data set, that non-zero values of α_z are of sub-photospheric origin [*Leka et al.,* 1996]. On the other hand, *van Driel Gesztelyi et al.* [1997] argued that currents may also be induced by sunspot motions.

Patterns in α_z probably exist throughout the lifetime of active regions – from emergence through decay. Figure 4 shows α_z maps of the AR NOAA 7926 during its dissipation. The pattern of α evolved only gradually over four days of observation. Using cross-correlation coefficients computed for each pair of magnetograms of the dataset we found a characteristic decay time of α_z

Figure 4

pattern $\tau \simeq 47$ hours, but visually the pattern can be identified over period of 4 days.

The α_z pattern shown on Figure 4 implies that oppositely directed and parallel electric currents flow inside the magnetic flux rope. However, one should expect the interaction between these currents (i.e. coalescence, [*Nishikawa et al.*, 1994]) to destroy the pattern.

To test this hypothesis we [*Pevtsov and Canfield*, 1998] computed maps of α_z for 30 active regions observed by Haleakala Stokes Polarimeter for at least 8 consecutive days. For these active regions we defined contours of α_z corresponding $\pm 1 \cdot 10^{-9} m^{-1}$ and studied the evolution of the area and value of α_z averaged over the area inside a contour. We found no systematic variation of these two parameters with active region age. On the other hand, the pattern does evolve over a few days. Hence, we concluded that α_z patterns observed in active regions evolve either as a result of rearrangement of individual patches or flux emergence; hence, they can be used to study subphotospheric processes.

If local photospheric helicity patterns originate in the convection zone, what can we learn about physical processes there? Numerical dynamo models [*Brummell et al.*, 1996] show that small scale flows with both signs of kinetic helicity develop in a dynamo region as a result of turbulent convection in a rotating coordinate system. These flows may generate magnetic fields with opposite twists, which one can observe in the photosphere.

Longcope et al. [1996] studied the evolution of a cross-section of an isolated flux tube rising through the convection zone and found that the interaction between the flux tube and its surroundings lead to bifurcation. The circulation twists each tube of the pair in an opposite sense. The amount of twist and the fragmentation scale depend on several parameters, including the vertical velocity, magnetic flux, viscosity and size. On the other hand, internal twist above a certain threshold stabilizes the flux tube [*Linton et al.*, 1996].

6. LARGE-SCALE HELICITY PATTERN

Several studies imply large-scale organization of fields and flows on scales larger than the size of a typical active region.

6.1. Clusters of Active Regions

Active regions tend to form in clusters or “nests” of activity that may last from three to six solar rotations [*Gaizauskas*, 1993]. Perhaps such persistent magnetic activity reflects dynamo processes, and hence can appear in helicity data as well. *Canfield and Pevtsov* [1998] studied the distribution of active regions with longitude and found that there are activity nests which maintain the same sign of helicity for several successive solar rotations. Figure 5 gives examples of these nests of helicity for Carrington rotations 1800–1985 (March 1988 – May 1995). The best example of such an area is seen in the northern hemisphere near 360°between solar rotations 1862–1870. The existence of nests of recurrent helicity has recently been confirmed by *Zhang and Bao* [1998].

Figure 5

Canfield and Pevtsov [1998] see persistence of the areas for several rotations as an indication that the helicity of the fields in these regions has been generated at great depths, not near the surface. The "helicity nests" may persist for up to 5 solar rotations, a few times longer than the theoretical estimates for the time a typical flux tube will rise from the bottom of the convection zone to the photosphere [*D'Silva and Howard*, 1994]. Hence they speculate that helicity nests may be the result of large-scale motions in the convection zone.

6.2. *Large-Scale Helicity Areas*

Latushko and Pevtsov [1998] studied the current helicity of the large-scale magnetic field, using WSO and MDI data (Section 3.2). Figure 6 shows their results for 5 successive solar rotations. The authors found large-scale areas of both positive and negative chirality in both hemispheres. Some areas persisted for several solar rotations (Fig. 6, examples 1-5), while individual active regions came and went (Fig. 6, examples 1 and 2).

Figure 6

Coronal data from the Soft-X ray Telescope on the Yohkoh spacecraft seems to support such large-scale helicity areas, albeit indirectly. *Sandborgh et al.* [1998] used Yohkoh SXT data to identify boundaries of independent coronal flux systems and their chirality (using sigmoidal loops). Examining 10 solar rotations, they found several such flux systems with a typical size of 30-60° persisting for up to 5 solar rotations. For further discussion of these results see *Canfield and Pevtsov* [1999].

Recently, giant convective cells were discovered [*Beck et al.*, 1998; *Hathaway et al.*, 1998]. The typical size of the convective cells is about 40°, and the individual cells persist for few solar rotations. Strikingly, the spatial and temporal scales of these features are very similar. We speculate that the large-scale helicity areas, coronal flux systems and giant convective cells may be simply different indications of same phenomenon.

7. DISCUSSION

Some researchers see the hemispheric helicity rule as an indication of sub-photospheric processes [*Rust and Kumar*, 1994; *Pevtsov et al.*, 1997]. Others see it as a result of large-scale photospheric shear motions [*Zirker et al.*, 1997; *Foukal*, 1997; *van Ballegooijen et al.*, 1998]. What is the relative importance of each of these mechanisms on the Sun? Is there some signature of large-scale circulation in Fig. 6?

The orientation of bipolar active regions and coronal arcades, with one polarity situated closer to the solar equator than the other, allows differential rotation to shear their magnetic fields and produce S-shaped coronal loops in southern hemisphere and inverse-S shapes in the northern [*van Ballegooijen et al.*, 1998]. By its nature, differential rotation and Coriolis force should produce repeatedly same sign of twist in same hemisphere and hence, a strong hemispheric rule. Apparently, both chirality of active regions and current helicity of large-scale magnetic field indicate that the rule is weak, *i.e.* there are areas of both sign of helicity in both hemispheres. We see the weakness of the hemispheric helicity rule as indirect evidence that neither differential rotation nor Coriolis force play a dominant role in creation of twist. As well, the local helicity pattern can not be understood in the framework of these two global mechanisms alone.

It appears that there is a certain disagreement between the Mees Solar Observatory HSP [*Pevtsov et al.*, 1995] and Huairou Solar Station [*Bao and Zhang*, 1998] datasets on the strength of the hemispheric helicity rule. The HSP has been used to study helicity via the α_{best}, the HSS employed current helicity H_c. Since for the force-free field $H_c = \alpha B^2$, both helicity proxies should have the same sign. Indeed, *Zhang and Bao* [1998] found that α and H_c correlate quite well with each other in their dataset. On the other hand, they found that the hemispheric helicity rule is much stronger in H_c data and weaker in α_{best}. We suspect that the presence of Faraday rotation in the HSS data may explain stronger hemispheric asymmetry in H_c (see Section 3.1.3 and *Hagyard et. al.* [1998]).

The interaction between magnetic field rising through the convection zone and the turbulent convection – the Σ-effect, [*Longcope et al.*, 1999] – can explain many observed features: weakness of the hemispheric helicity rule, large scatter in Fig. 1, the typical value of α_{best}. It also can explain the local helicity pattern. On the other hand, the observed tilt-twist correlation [*Canfield and Pevtsov*, 1998] suggests that at least some amount of twist originates in the dynamo region.

Large-scale helicity areas open another challenge for helicity studies. If such areas do exist, do they reflect large-scale circulation in the dynamo region? What is importance of such circulation on the dynamo? The study of large-scale helicity areas is in its infancy. Although the preliminary results are interesting, it would be premature to make serious conclusions based on them.

Acknowledgments. We are grateful to Dr. S.M. Latushko for providing us with the data for Figure 2. This research has been supported by NASA through SR&T grant NAG5-5043 and the Yohkoh Soft X-Ray Telescope contract NAS8-40801.

REFERENCES

Abramenko, V. I., Wang, T., and Yurchishin, V. B., Electric current helicity in 40 active regions in the maximum of solar cycle 22, *Solar Phys.*, *174*, 291–296, 1997.

Babcock, H., The topology of the Sun's magnetic field and the 22-year cycle, *Astrophys. J.*, *304*, 542–559, 1961.

Bao, S. and Zhang, H., Patterns of current helicity for the twenty-second solar cycle, *Astrophys. J.*, *496*, L43–L46, 1998.

Beck, J. G., Duvall, T. L., Scherrer, P. H., and Hoeksema, J. T., The detection of giant velocity cells on the Sun (abstract), *Eos Trans. AGU*, *79*(17), Spring Meet. Suppl., S281, 1998.

Brummell, N. H., Hurlburt, N. E., and Toomre, J., Turbulent compressible convection with rotation. I. Flow structure and evolution, *Astrophys. J.*, *473*, 494–513, 1996.

Canfield, R. C. and Pevtsov, A. A., Helicity of solar active-region magnetic fields, in *Synoptic Solar Physics, A.S.P Conf. Ser.*, edited by K.S. Balasubramaniam, J.W. Harvey and M. Rabin, *140*, pp. 131–143, A.S.P., 1998.

Canfield, R. C. and Pevtsov, A. A., Helicity and reconnection in the solar corona: observations, in *Magnetic Helicity in Space and Laboratory Plasmas*, edited by M.R. Brown, R.C. Canfield and A.A. Pevtsov, Geophys. Monogr. Ser., AGU, Washington, D.C., this volume, 1999.

D'Silva, S. and Howard, R. F., Sunspot rotation and the field strengths of subsurface flux tubes, *Solar Phys.*, *151*, 213–230, 1994.

Duvall, T., Scherrer, P. H., Svalgaard, L., and Wilcox, J., Average photospheric poloidal and toroidal magnetic field components near solar minimum, *Solar Phys.*, *61*, 233–245, 1979.

Field, G., Magnetic helicity in astrophysics, in *Magnetospheric phenomena in astrophysics*, pp. 324–341, American Institute of Physics, New York, 1986.

Fisher, G. H., Fan, Y., and Howard, R. F., Comparisons between theory and observations of active region tilts, *Astrophys. J.*, *438*, 463–471, 1995.

Foukal, P., Chirality, helicity, and Joy's law, in *New Perspectives on Solar Prominences, Proceedings of a meeting held in Aussois, France (IAU Colloquium 167) 28 April -4 May 1997*, pp. 446, 1998.

Gaizauskas, V., *Adv. Space Res.*, *12*(9), 5, 1993.

Gary, G. A., Moore, R. L., Hagyard, M. J., and Haisch,

B. M., Nonpotential features observed in the magnetic field of an active region, *Astrophys. J.*, *314*, 782–794, 1987.

Grigoryev, V. M. and Latushko, S. M., E-W motions of large-scale magnetic field structures of the Sun, *Solar Phys.*, *140*, 239–245, 1992.

Hagyard, M. J., Cumings, N. P., and West, E. A., The MSFC vector magnetograph, in *Proceedings of Kunming Workshop on Solar Physics and Interplanetary Traveling Phenomena*, edited by C. De Jager and Chen Biao, pp. 204–204, Science Press, Beijing, China, 1985.

Hagyard, M. J., Pevtsov, A. A., and Canfield, R. C., Studies of solar magnetic helicity with the MSFC vector magnetograph, *Solar Phys.*, in preparation, 1998.

Hale, G. E., The fields of force in the atmosphere of the Sun, *Nature*, *119*(3002), 708–714, 1927.

Hathaway, D. H., Bogart, R. S., and Beck, J. G., A search for giant cells on the Sun (abstract), *Eos Trans. AGU*, *79*(17), Spring Meet. Suppl., S281, 1998.

Latushko, S. M. and Pevtsov, A. A., in preparation, *Astrophys. J.*, 1998.

Leka, K. D., Canfield, R. C., McClymont, A. N., and Van Driel-Gesztelyi, L., Evidence for current-carrying emerging flux, *Astrophys. J.*, *462*, 547–560, 1996.

Linton, M. G., Longcope, D. W., and Fisher, G. H., The helical kink instability of isolated, twisted magnetic flux tubes, *Astrophys. J.*, *469*, 954–963, 1996.

Lites, B. W., Elmore, D. F., Seagraves, P., and Skumanich, A. P., Stokes profile analysis and vector magnetic fields. VI. Fine scale structure of a sunspot, *Astrophys. J.*, *418*, 928–942, 1993.

Longcope, D. W. and Fisher, G. H., The effect of convection zone turbulence on a rising flux tube, *Astrophys. J.*, *458*, 380–390, 1996.

Longcope, D. W., Fisher, G. H., and Pevtsov, A. A., Flux tube twist resulting from helical turbulence: the Σ-effect, *Astrophys. J.*, *507*, 417–432, 1998.

Longcope, D., Linton, M., Pevtsov, A., Fisher, G., and Klapper, I., Twisted flux tubes and how they get that way, in *Magnetic Helicity in Space and Laboratory Plasmas*, edited by M.R. Brown, R.C. Canfield and A.A. Pevtsov, Geophys. Monogr. Ser., AGU, Washington, D.C., this volume, 1999.

Martin, S. F., Bilimoria, R., and Tracadas, P. W., Magnetic field configurations basic to filament channels and filaments, in Rutten, C. J. and Schrjiver, C. J. (Eds.), *Solar Surface Magnetism*, pp. 303–338, Kluwer Academic Publishers, Dordrecht, 1994.

Mickey, D. L., The Haleakala stokes polarimeter, *Solar Phys.*, *97*, 223–238, 1985.

Moffatt, H. K. and Ricca, R. L., Helicity and the Călugăreanu invariant, *Proc. R. Soc. Lond. A*, *439*, 411–429, 1992.

Nishikawa, K. I., Sakai, J. I., Zhao, J., Neubert, T., and Buneman, O., Coalescence of two current loops with a kink instability simulated by a three-dimensional electromagnetic particle code, *Astrophys. J.*, *434*, 363–369, 1994.

Pevtsov, A. A. and Canfield, R. C., *Astrophys. J.*, *in preparation* 1998.

Pevtsov, A. A., Canfield, R. C., and McClymont, A. N., On the subphotospheric origin of coronal electric currents, *Astrophys. J.*, *481*, 973–977, 1997.

Pevtsov, A. A., Canfield, R. C., and Metcalf, T. R., Patterns of helicity in solar active regions, *Astrophys. J.*, *425*, L117–L119, 1994.
Pevtsov, A. A., Canfield, R. C., and Metcalf, T. R., Latitudinal variation of helicity of photospheric magnetic fields, *Astrophys. J.*, *440*, L109–L112, 1995.
Pevtsov, A. A. and Latushko, S. M., Helicity of large scale photospheric magnetic fields (abstract), *Bull. Amer. Astron. Soc.*, *27*(2), 978, 1995.
Pevtsov, A. A. and Peregud, N. L., Electric currents in a unipolar sunspot, in *Physics of Magnetic Flux Ropes*, edited by C.T. Rassel, E.R. Priest and L.C. Lee, Geophys. Monogr. Ser., *58*, pp. 161–165, AGU, Washington, D.C., 1990.
Priest, E. R., *Solar magnetohydrodynamics*, Reidel, Dordrecht 1984.
Richardson, R. S., The nature of solar hydrogen vortices, *Astrophys. J.*, *93*, 24–28, 1941.
Rust, D. M., Magnetic helicity in solar filaments and coronal mass ejections, in *Magnetic Helicity in Space and Laboratory Plasmas*, edited by M.R. Brown, R.C. Canfield and A.A. Pevtsov, Geophys. Monogr. Ser., AGU, Washington, D.C., this volume, 1999.
Rust, D. M. and Kumar, A., Helical magnetic fields in filaments, *Solar Phys.*, *155*, 69–97, 1994.
Rust, D. M. and Kumar, A., Evidence for helically kinked magnetic flux ropes in solar eruptions, *Astrophys. J.*, *464*, L199–L202, 1996.
Sandborgh, S. C., Canfield, R. C., and Pevtsov, A. A., Chirality of large-scale flux systems in the solar corona (abstract), *Eos Trans. AGU*, *79*(17), Spring Meet. Suppl., S285, 1998.
Seehafer, N., Electric current helicity in the solar atmosphere, *Solar Phys.*, *125*, 219–232, 1990.
Semel, M., Mouradian, Z., Soru-Escaut, M., Maltby, P., Rees, D., Makita, M., and Sakurai, T., Active regions, sunspots and their magnetic fields, in *Solar Interior and Atmosphere*, edited by A. Cox, W. Livingston, and M. Matthews, pp. 844–889, The University of Arizona Press, Tucson, 1991.
Skumanich, A. and Lites, B. W., Stokes profile analysis and vector magnetic fields. I - Inversion of photospheric lines, *Astrophys. J.*, *322*, 473–482, 1987.
Stenflo, J. O., *Solar Magnetic Fields, Polarized Radiation Diagnostics*, Kluwer Academic Publishers, Dordrecht, 1994.
Van Ballegooijen, A. A., Cartledge, N. P., and Priest, E. R., Magnetic flux transport and the formation of filament channels on the Sun, *Astrophys. J.*, *501*, 866–881, 1998.
Van Driel-Gesztelyi, L., Csepura, G., Schmieder, B., Malherbe, J. M., and Metcalf, T., Evolution of a delta group in the photosphere and corona, *Solar Phys.*, *172*, 151–160, 1997.
West, E. A. and Hagyard, M. J., Interpretation of vector magnetograph data including magneto-optic effects. I - Azimuth angle of the transverse field, *Solar Phys.*, *88*, 51–64, 1983.
Zhang, H. and Bao, S., private communication, 1998.
Zirin, H., *Astrophysics of the Sun*, Cambridge Univ. Press, Cambridge, 1988.
Zirker, J. B., Martin, S. F., Harvey, K. H., and Gaizauskas, V., Global magnetic patterns of chirality, *Solar Phys.*,

175, 45–58, 1997.

A. A. Pevtsov, R. C. Canfield, Department of Physics, Montana State University, P.O. Box 173840, Bozeman, MT 59717-3840. (e-mail: pevtsov@physics.montana.edu; canfield@physics.montana.edu)

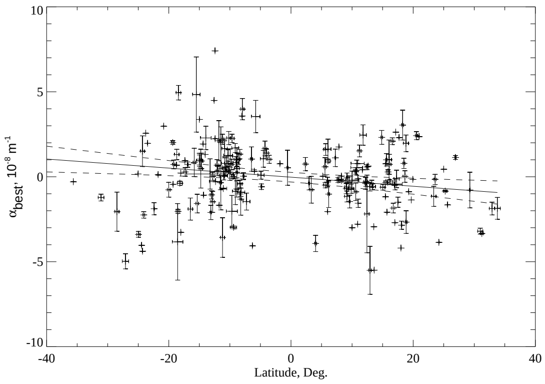

Figure 1. Values of α_{best} for 203 active regions. Error bars reflect the variation in α_{best} from independent measurements of the same AR. A linear fit to the data is shown by the solid line, two dashed lines show 2σ errors of the fit. By permission [*Longcope et al.*, [1998]

Figure 1. Values of α_{best} for 203 active regions. Error bars reflect the variation in α_{best} from independent measurements of the same AR. A linear fit to the data is shown by the solid line, two dashed lines show 2σ errors of the fit. By permission [*Longcope et al.*, [1998]

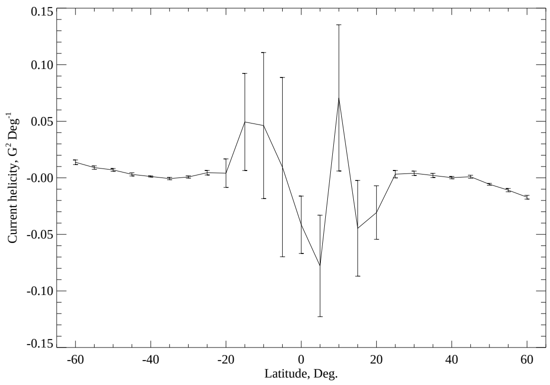

Figure 2. Variation of the current helicity H_c of large-scale magnetic field with solar latitude computed using 184 arc. sec spatial averaging. Error bars refer to 1 σ of computational error.

Figure 2. Variation of the current helicity H_c of large-scale magnetic field with solar latitude computed using 184 arc. sec spatial averaging. Error bars refer to 1 σ of computational error.

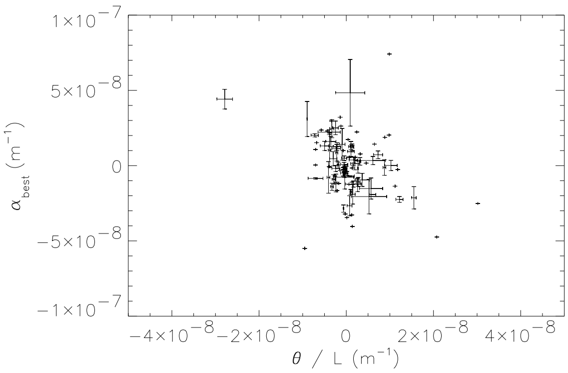

Figure 3. The dependence of observed active region α_{best} on the ratio of tilt to characteristic length.

Figure 3. The dependence of observed active region α_{best} on the ratio of tilt to characteristic length.

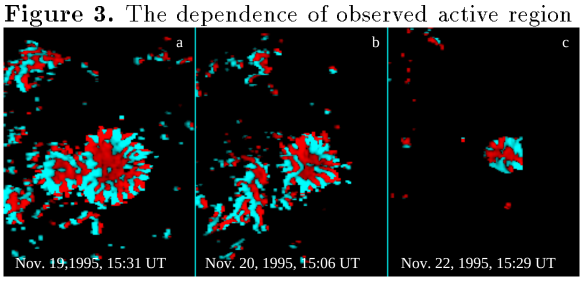

Figure 4. Local helicity (α_z) pattern of dissipating sunspot of AR NOAA 7926 from Advanced Stokes Polarimeter (ASP) observations. Dark grey color indicates positive α_z, light grey indicates negative α. Pixels below noise level are shown in black (see Sec. 5).

Figure 4. Local helicity (α_z) pattern of dissipating sunspot of AR NOAA 7926 from Advanced Stokes Polarimeter (ASP) observations. Dark grey color indicates positive α_z, light grey indicates negative α. Pixels below noise level are shown in black (see Sec. 5).

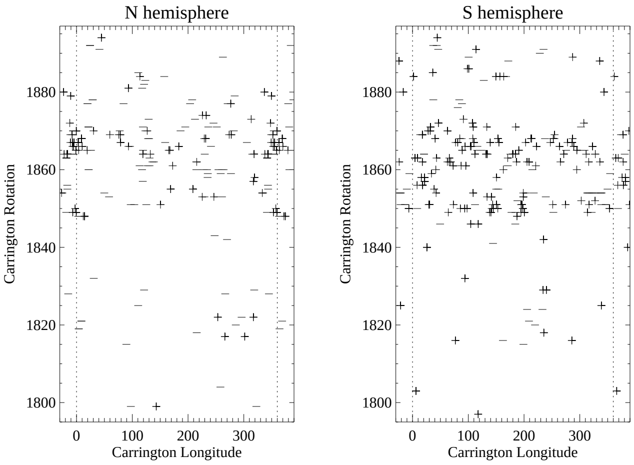

Figure 5. Carrington longitude-rotation charts for the northern (left) and southern (right) hemispheres. The + and - symbols indicate the sign of α_{best} for the active region.

Figure 5. Carrington longitude-rotation charts for the northern (left) and southern (right) hemispheres. The + and - symbols indicate the sign of α_{best} for the active region.

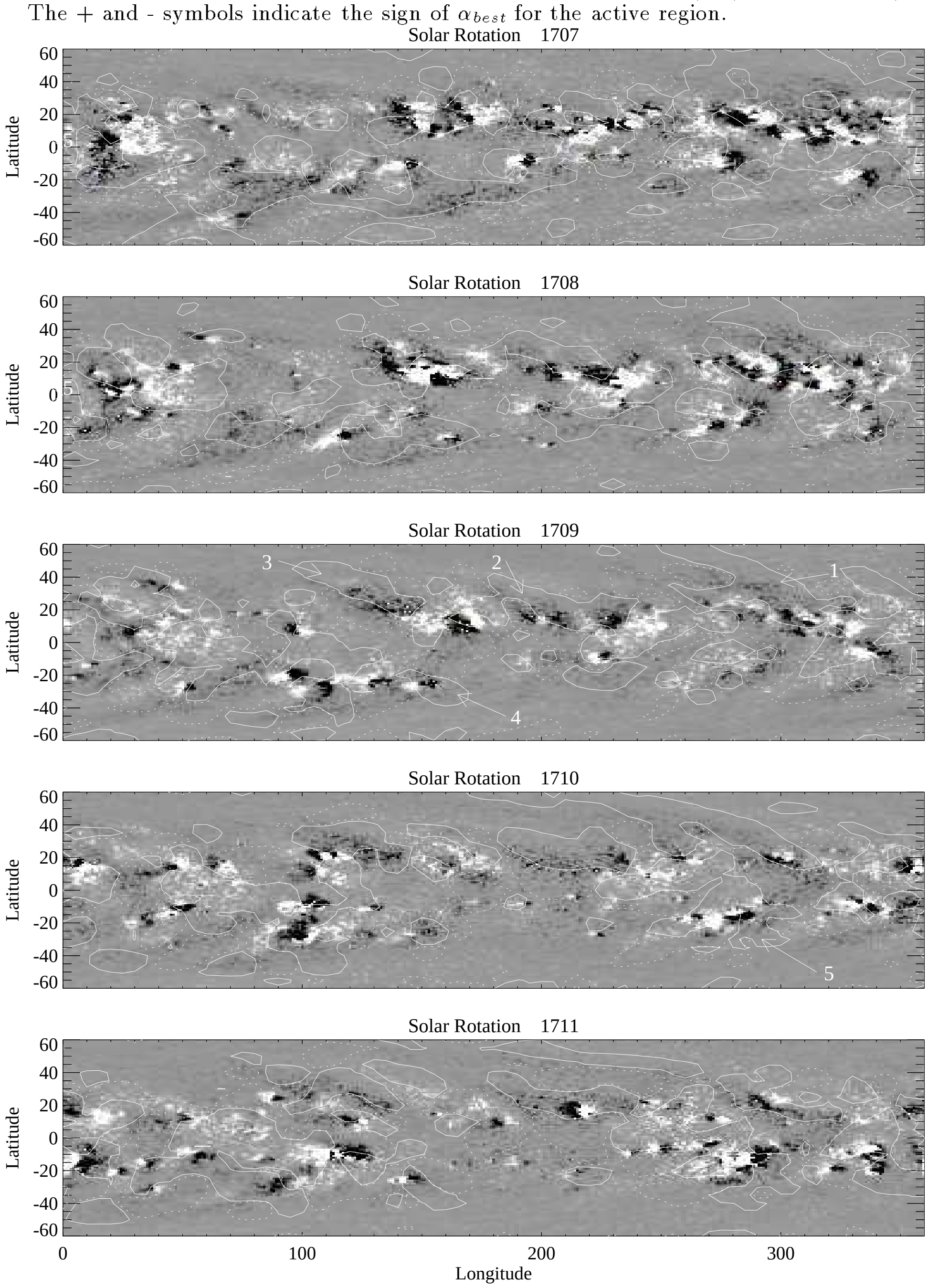

Figure 6. Carrington maps of contours of current helicity density ($\mathbb{H}_c = B_z \cdot (\nabla \times B)_z$) derived using daily full disk WSO magnetograms for the period of April – August 1981. Contours show levels of $\pm$ 500 μT^2 degree^{-1} with solid contours showing positive and dashed - showing negative values. The underlying images are synoptic KPNO magnetograms. White indicates positive polarity (see Sec. 6).

Figure 6. Carrington maps of contours of current helicity density ($\mathrm{H}_c = B_z \cdot (\nabla \times B)_z$) derived using daily full disk WSO magnetograms for the period of April – August 1981. Contours show levels of $\pm$ 500 $\mu\mathrm{T}^2$ degree^{-1} with solid contours showing positive and dashed - showing negative values. The underlying images are synoptic KPNO magnetograms. White indicates positive polarity (see Sec. 6).

Table 1. Sign of α_{best} for 203 Active Regions

	Negative	Positive	Total
N hemisphere	58[a](62%)[b]	35 (38%)	93
S hemisphere	37 (34%)	73 (66%)	110
Total	95	108	203

[a]Absolute number of active regions
[b]Percent of active regions in the hemisphere

HELICITY OF THE PHOTOSPHERIC MAGNETIC FIELD

PEVTSOV & CANFIELD

HELICITY OF THE PHOTOSPHERIC MAGNETIC FIELD

PEVTSOV & CANFIELD

HELICITY OF THE PHOTOSPHERIC MAGNETIC FIELD

PEVTSOV & CANFIELD

HELICITY OF THE PHOTOSPHERIC MAGNETIC FIELD

PEVTSOV & CANFIELD

HELICITY OF THE PHOTOSPHERIC MAGNETIC FIELD

PEVTSOV & CANFIELD

HELICITY OF THE PHOTOSPHERIC MAGNETIC FIELD

PEVTSOV & CANFIELD

HELICITY OF THE PHOTOSPHERIC MAGNETIC FIELD

PEVTSOV & CANFIELD

HELICITY OF THE PHOTOSPHERIC MAGNETIC FIELD

PEVTSOV & CANFIELD

HELICITY OF THE PHOTOSPHERIC MAGNETIC FIELD

PEVTSOV & CANFIELD

HELICITY OF THE PHOTOSPHERIC MAGNETIC FIELD

PEVTSOV & CANFIELD

HELICITY OF THE PHOTOSPHERIC MAGNETIC FIELD

PEVTSOV & CANFIELD

HELICITY OF THE PHOTOSPHERIC MAGNETIC FIELD

PEVTSOV & CANFIELD

HELICITY OF THE PHOTOSPHERIC MAGNETIC FIELD

PEVTSOV & CANFIELD

HELICITY OF THE PHOTOSPHERIC MAGNETIC FIELD

PEVTSOV & CANFIELD

HELICITY OF THE PHOTOSPHERIC MAGNETIC FIELD

PEVTSOV & CANFIELD

HELICITY OF THE PHOTOSPHERIC MAGNETIC FIELD

PEVTSOV & CANFIELD

HELICITY OF THE PHOTOSPHERIC MAGNETIC FIELD

PEVTSOV & CANFIELD

HELICITY OF THE PHOTOSPHERIC MAGNETIC FIELD

PEVTSOV & CANFIELD

HELICITY OF THE PHOTOSPHERIC MAGNETIC FIELD

PEVTSOV & CANFIELD